journal

J. Am. Ceram. Soc., 78 [7] 1940–46 (1995)

Molten Glass Corrosion Resistance of Immersed Combustion-Heating Tube Materials in E-Glass

S. Kamakshi Sundaram,* Jen-Yen Hsu,* and Robert F. Speyer*

School of Materials Science and Engineering, Georgia Institute of Technology, Atlanta, Georgia 30332-0245

The corrosion resistance of molybdenum, molybdenum disilicide, and a $SiC_{(p)}/Al_2O_3$ composite to molten E-glass at 1550°C was studied. Mo showed no tendency to oxidize as it was immersed in soda–lime silicate glass in a parallel study. $MoSi_2$ was corroded by soluble molecular oxygen, leaving a Mo_5Si_3 interface behind. The $SiC_{(p)}/Al_2O_3$ composite was corroded at a more rapid rate wherein the SiC component was oxidized to form amorphous silica and CO bubbles. Based on these results, the activity of soluble molecular oxygen in E-glass was determined to be in the range of 2.4×10^{-14} to 2.0×10^{-8}.

I. Introduction

The work discussed herein is part of a larger research thrust to develop materials for immersed gas-fired radiant burner tubes for glass melters. In the evaluation of candidate materials, our research has adopted a parallel approach, separately evaluating molten glass corrosion and combustion gas corrosion, as well as using thermodynamic simulations for both processes. Gas corrosion investigations are reported elsewhere.[1,2] In the present paper, the corrosion resistance of candidate materials to a molten E-glass (fiberglass) composition is presented.

Of the candidate materials evaluated, those presented here are molybdenum, molybdenum disilicide, and a $SiC_{(p)}/Al_2O_3$ composite (p refers to particulate). Molybdenum has been used as the electrode material for electric melting and boosting in glass-melting tanks for many years.[5,6] Molybdenum disilicide has demonstrated a self-protective mechanism of forming an amorphous SiO_2 layer at the surface in an oxidizing atmosphere.[7] In the case of the $SiC_{(p)}/Al_2O_3$ composite, the combination of high thermal conductivity of SiC and the refractory properties of Al_2O_3 was anticipated to make it suitable for the combustion product side of the present application. This work closely parallels corrosion studies of these candidate materials in soda–lime–silicate glass at 1565°C.[3] In that work, all three materials were found to corrode by oxidation reactions. An oxidation product interfacial region of $MoO_{2(s)}$ for Mo, and Mo_5Si_3 for $MoSi_2$, formed, which periodically cracked away due to interfacial stresses. CO/CO_2 bubbles formed as a reaction product in the corrosion of the $SiC_{(p)}/Al_2O_3$ composite.

II. Experimental Procedure

The ASTM standard method C621-84 for isothermal corrosion resistance of refractories to molten glass was revised for the present investigation.[4] Since molybdenum oxidizes and volatilizes above the glass line at temperatures exceeding ~600°C, it was fully immersed. Soluble silicon in the melt, originating from $MoSi_2$ or $SiC_{(p)}/Al_2O_3$, alloys with platinum to destroy the crucible. Therefore, fusion-cast AZS (UNICOR501, Corhart Refractories, Louisville, KY) crucibles with containment volumes of 3.81 cm diameter by 3.81 cm depth were used. AZS consists of 50.80 wt% Al_2O_3, 32.60 wt% ZrO_2, 14.90 wt% SiO_2, 1.25 wt% Na_2O, 0.13 wt% Fe_2O_3, and 0.12 wt% TiO_2.[9]

Molybdenum (Johnson Matthey/AESAR, Ward Hill, MA) specimens were of 12.5 mm diameter by 12.5 mm length for the purpose of complete immersion. Chemical analysis for trace elements in as-received molybdenum showed less than 1 ppm of Al, Ca, Cr, Cu, Mg, Mn, Ni, Pb, Si, Sn, and Ti, less than 2 ppm of C and O, and less than 14 ppm of Fe. Cylindrical specimens of $MoSi_2$ (Kanthal Super 33, Kanthal, Bethel, CT) and $SiC_{(p)}/Al_2O_3$ (DuPont-Lanxide™ Composites, Wilmington, DE) of 12.5 mm diameter by 60 mm length were used. As determined by scanning electron microscopy (SEM) image analysis, the as-received $MoSi_2$ contained 1.7 vol% Mo_5Si_3 grains, generally in contact with amorphous aluminosilicate glassy pockets, which in turn comprised 18.6 vol% of the specimen.

The E-glass (Owens/Corning Fiberglas, Granville, OH) used in the present investigation is a common fiberglass composition. A chemical analysis of the as-received glass, in weight percent, shows SiO_2 = 54.4%, CaO = 17.9%, Al_2O_3 = 14.7%, B_2O_3 = 6.3%, MgO = 4.7%, Na_2O = 0.6%, TiO_2 = 0.6%, F_2 = 0.5%, and Fe_2O_3 = 0.33%.

The as-received glass was crushed to −40 mesh, and the AZS crucible with 48.5 g of glass was placed inside an electrically heated furnace. The glass was heated to 1550°C and allowed to equilibrate at that temperature for 2 h to obtain bubble-free glass. Test specimens were then loaded into the crucible and exposed for 12, 24, or 48 h. Details of measurement and characterization procedures may be found in related published work.[3,8]

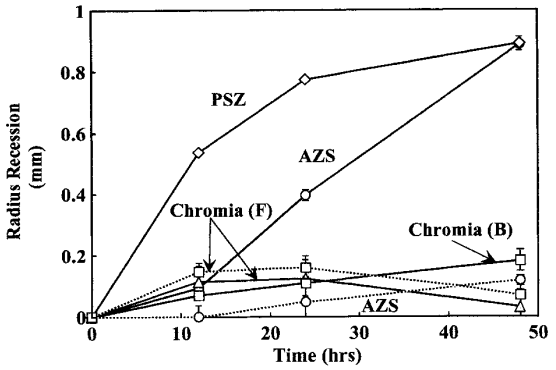

Fig. 1. Corrosion of refractory containment materials at glass-line (solid lines) and half-down (dotted lines) regions. The error bars indicate the standard deviation in the measurement of specimen diameters before the corrosion tests.

J. L. Smialek—contributing editor

Manuscript No. 194582. Received May 10, 1993; approved February 16, 1995.
Supported by the Gas Research Institute under Contract No. 5090-298-2073. Much of this work was performed at the New York State College of Ceramics at Alfred University.
*Member, American Ceramic Society.

Table I. Chemical Analyses (wt%) of Glass after Interaction with AZS at 1550°C

Corrosion time (h) = 0	3	6	12	24	36	48
SiO_2 54.4	53.8	54.8	54.5	53.5	54	53.2
Al_2O_3 14.7	15.7	15.6	15.7	17.4	17.2	18.1
ZrO_2 0	0	0	0	0.15	0.55	1.01

III. Results and Discussion

The choice of AZS was made after static corrosion testing of fusion-cast AZS, MgO-partially-stabilized zirconia (PSZ) (Coors Ceramics, Golden, CO), fusion-cast chromia (Carborundum, Monofrax Refractories Division, Falconer, NY), and bonded chromia (Corhart Refractories, Buchannon, WV) refractories, following the ASTM C621-84 standard. The results of corrosion testing, presented in Fig. 1, indicate that AZS had an inferior corrosion resistance, both at the glass line and half-down regions, to bonded and fusion-cast chromia. The half-down corrosion rates of bonded chromia and PSZ could not be measured due to specimen cracking, for the latter, undoubtedly from destabilization of the cubic crystal structure. Fusion-cast chromia demonstrated slight recession up to 24 h, followed by an apparent increase in cross-sectional area after 48 h of exposure. This remarkable feature consistently appeared during three separate trials, in both half-down and glass-line measurements. Two possibilities are suggested: (1) The high vapor pressure of chromia tended to expand porous regions and increased specimen dimensions by creep. (2) The chemistry of solid solutions within the refractory changed via incorporation of ions from the glass into the chromia structure, in turn causing a volume expansion. Bonded chromia did not show this dilation behavior. AZS refractory was, nevertheless, selected as the containment material over chromia refractories, to eliminate glass coloration.

The chemical analyses of the glass after interaction with AZS for varying times are shown in Table I. No significant changes in these constituents were observed up to 12 h of exposure. Beyond 12 h, the Al_2O_3 and ZrO_2 content increased; after 48 h of exposure, the Al_2O_3 weight fraction increased to 2.4%, and ZrO_2 to 1.01%. The effect of this compositional change on the specimen corrosion rate is not known. Replenishing glass melt after every 12 h of exposure was considered and rejected, since it changes the present static testing to a semidynamic corrosion test.

Figures 2(a and b) show the corrosion of cylindrical specimens by molten glass (in turn contained in AZS crucibles). In the case of glass-line corrosion, $SiC_{(p)}/Al_2O_3$ showed a corrosion rate comparable to that of $MoSi_2$ for the first 24 h but accelerated beyond that. $SiC_{(p)}/Al_2O_3$ corrosion appeared largely independent of positioning at the glass-line or half-down locations. $MoSi_2$ showed an order of magnitude decrease in recession rate at the half-down position as compared to the glass-line position. Immersed Mo showed the least corrosion, with no measurable corrosion for the first 24 h.

(1) Molybdenum

Figure 3 shows the Mo–glass interfacial morphology; no interfacial layer can be seen. This is corroborated by a line EDS scan (not shown) in which a sharp decrease in Mo concentration with corresponding sharp increase in Si concentration was observed at the interface. XRD patterns starting from the glass side, penetrating into the bulk (not shown), did not show any interfacial phase at the Mo–glass interface.

Neither MoO_2 nor $MoO_{3(s)}$ were detected at the interfacial region. For the equilibria,

$$Mo_{(s)} + O_{2(glass)} = MoO_{2(s)}$$

$\Delta G^{\circ}_{1823K} = -268.6$ kJ/mol, $a_{O_{2(glass)}} = 2.0 \times 10^{-6}$. Thus, the molecular oxygen activity in the molten glass would have to be greater than or equal to 2.0×10^{-8} for this reaction to be favorable. The oxygen activity would have to equal or exceed 7.4×10^{-6} for $MoO_{3(g)}$ to be favorable.

The concentration of molecular oxygen in alkali silicate melts has been shown[10] to be 1% of that in the atmosphere, which translates to a soluble molecular oxygen activity of $\sim 2 \times 10^{-3}$ for glass in an air atmosphere. This was consistent with an observed MoO_2 surface layer on Mo exposed to molten soda–lime–silicate glass,[3] since this oxygen activity was well above the critical value of 2.0×10^{-8}. No information is available for the solubility of molecular oxygen in calcium aluminosilicates such as the E-glass composition studied herein. However, based on the fact that no molydenum oxides were observed, an oxygen activity below 2.0×10^{-8} at 1550°C in E-glass is indicated, assuming that there were no kinetic hindrances to oxide formation.

The enhancement in Mo corrosion between 24 and 48 h of exposure is suspected to be a result of solution of impurity phases from the AZS crucible. The presence of impurity phases such as As_2O_3, Na_2SO_4 have been shown[11] to enhance the corrosion of molybdenum in molten glass, but these phases are not present in AZS. However, solution of zirconia, iron oxide and

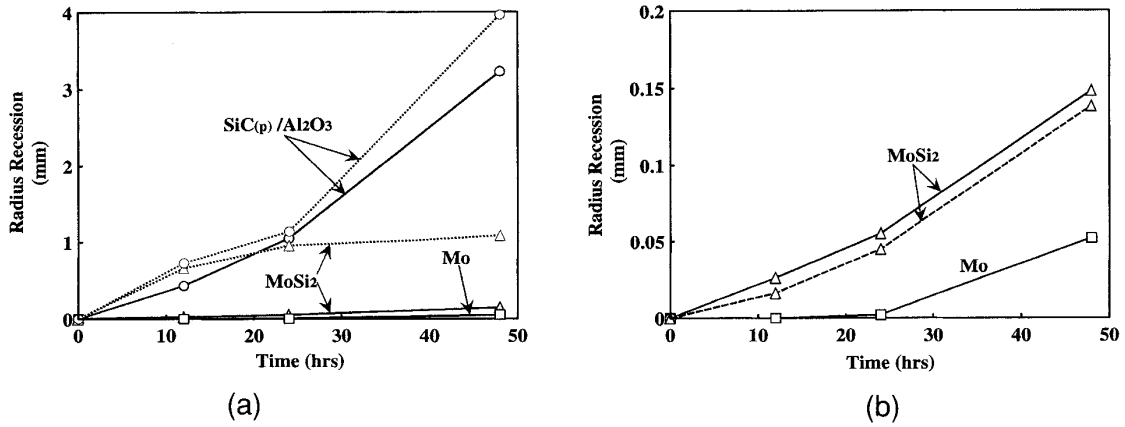

Fig. 2. (a) Specimen corrosion at the glass-line (dotted lines) and half-down regions (solid lines). (b) Magnified view of corrosion of half-down Mo and $MoSi_2$. Propagated error calculations[8] result in error bars smaller than the symbol size and are therefore not shown. The dashed line shows radius

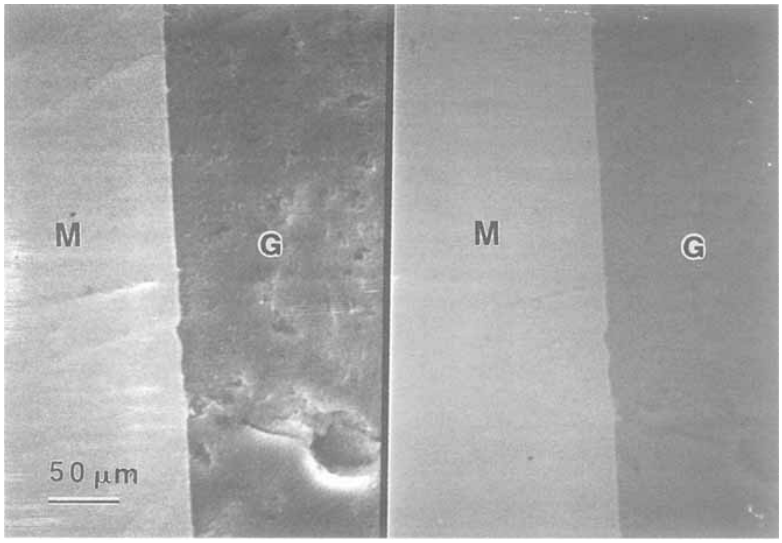

Fig. 3. Molybdenum–glass interfacial region after 48 h of corrosion. M: molybdenum, G: glass. Left: secondary electron image. Right: backscattered image.

titania, present in AZS, would be expected to alter the solubility of molecular oxygen in the glass. It is therefore possible that corrosion of the AZS crucible would cause the corrosion of Mo by increasing the solubility of molecular oxygen in E-glass.

(2) Molybdenum Disilicide

The as-received $MoSi_2$ had a fused silica surface layer of ~10 μm thickness. After preheat treatment at 1000°C for 10 min, the surface layer became somewhat thinner and discontinuous. If it is assumed that this vitreous coating mixed with the glass so that it was effectively removed, then the measured postcorrosion specimen radii would be affected, but not the trend in radius recession with exposure time. The dashed line in Fig. 2(b) shows the measured $MoSi_2$ specimen radii after subtraction of a 10 μm surface layer.

Figure 4 shows XRD patterns starting from the glass, penetrating through the interface, into the bulk. From the nearby glass to the interfacial region, molybdenum was identified. The major interfacial phase was identified to be Mo_5Si_3. Minor quantities of Mo_3Si could not be confirmed or denied, since the most intense peaks of this phase overlap with those of Mo_5Si_3.

An SEM EDS pattern was taken (not shown) of the surface from which the XRD second from the front in Fig. 4 was taken. Compared to as-received $MoSi_2$, appreciable molybdenum enhancement relative to silicon was apparent, corresponding to an XRD pattern showing predominantly Mo_5Si_3.

Figures 5(a and b) show the $MoSi_2$–glass interfacial features at the glass-line and half-down regions, respectively. The interfacial layer had a thickness of 133.2 ± 4.3 μm at the half-down region, and 13.0 ± 3.2 μm at the glass-line region. From the backscattered images, the interfacial region was richer in atomically heavier atoms. Since oxygen is lighter than both metals, the interfacial region is not an oxide such as MoO_2 or SiO_2. Mo being heavier than Si, the interfacial region is interpreted to be Mo-rich. Further corroboration is provided by EDS line scans (Fig. 6). At the interface, the Si-to-Mo ratio is decreased. Although the Si intensity varies throughout the interfacial region, a general Si concentration gradient from

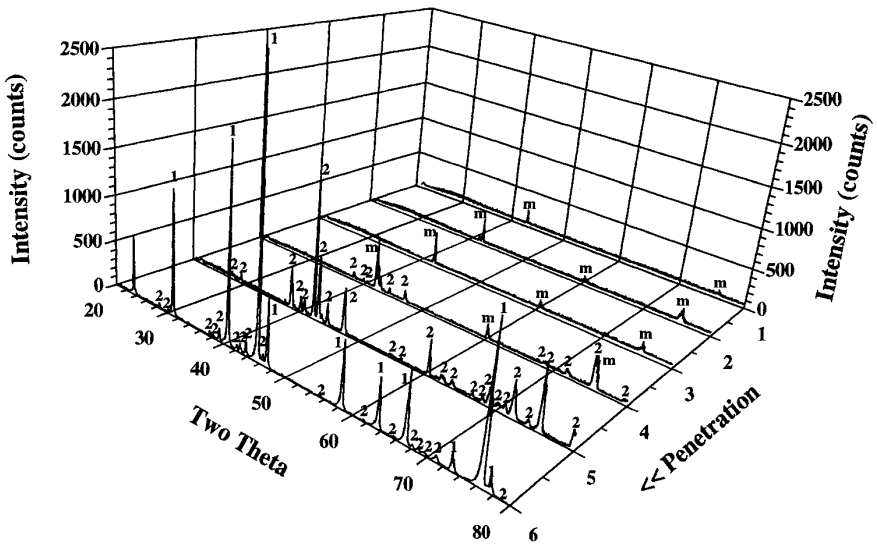

Fig. 4. XRD patterns as a function of penetration, analyzing glass, interfacial region, and molybdenum disilicide bulk. m: molybdenum, 1: $MoSi_2$

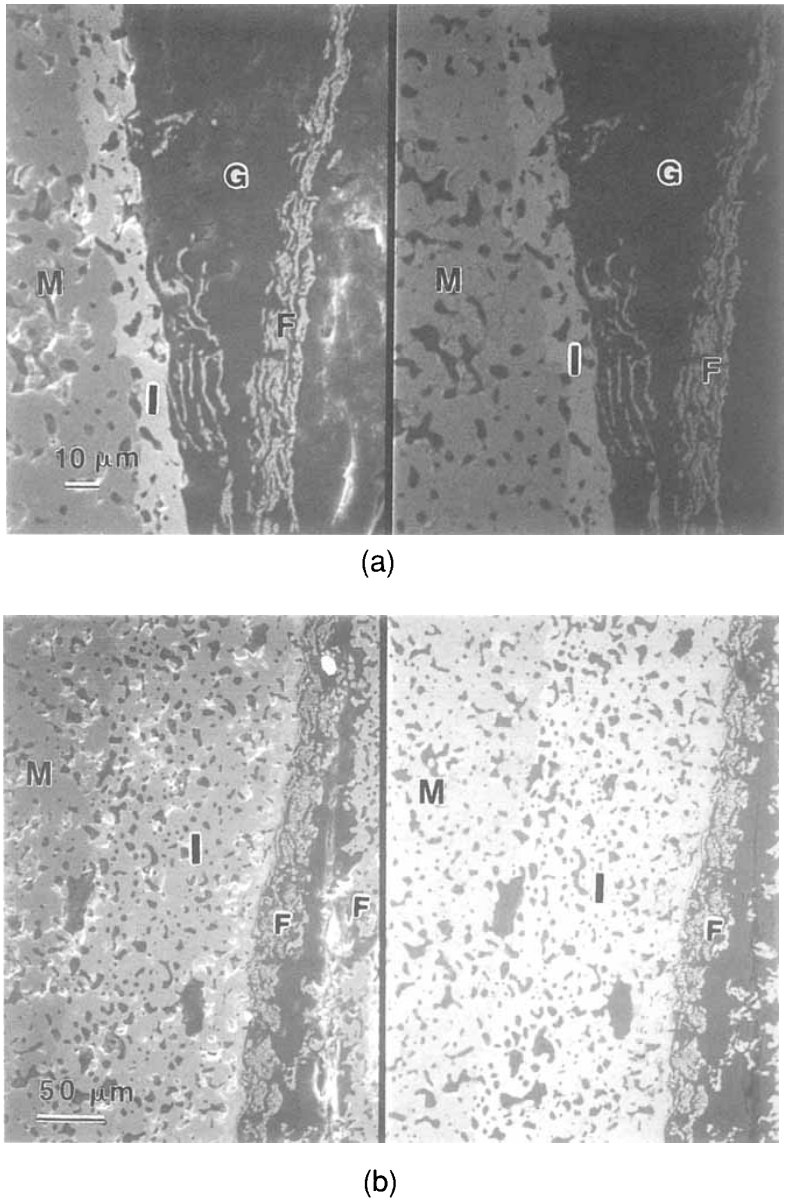

Fig. 5. Molybdenum disilicide–glass interfacial region at (a) glass-line and (b) half-down regions after 48 h of corrosion. M: molybdenum disilicide, I: interface, F: flaked-off layer, and G: glass. Left: secondary electron image. Right: backscattered image.

interior to exterior is apparent. The fluctuations in Si and Mo concentrations in the $MoSi_2$ bulk, as well as the interfacial region, are attributed to dispersed pockets of amorphous aluminosilicate phase throughout the material. A small Mo EDS peak away from the interface suggests a limited molybdenum-rich waste stream into the glass. As implied from Fig. 5, at the glass line, the flaked-off reaction-product layer was drawn away from the interface by enhanced glass-line convection currents.[12] This corrosion product layer remained close to the interface at the half-down region. This also explains the decreased interfacial layer thickness at the glass line as compared to the half-down region.

XRD, SEM, and EDS results provide conclusive evidence that the mechanism of $MoSi_2$ corrosion is removal of silicon from $MoSi_2$ to the glass, leaving a silicon-deficient molybdenum silicide interface. This is an oxidation reaction where oxygen was provided from soluble molecular oxygen: $5MoSi_2 +$

for equilibria of interest among compounds of Mo, Si, and O. As implied by the lowest standard free-energy equilibria line, formation of silica from $MoSi_2$ via the most oxygen conservative mechanism is favored—silica is formed by oxidation and removal of silicon from $MoSi_2$ to form Mo_5Si_3, rather than complete oxidation of the silicon component, the molybdenum component, or both. In addition, the most favored reaction is that most conservative in silicon removal from the compound; e.g., Mo_5Si_3 formed rather than Mo_3Si or Mo. If no $MoSi_2$ is locally available, then it would be thermodynamically favorable for Mo_5Si_3 to convert to Mo_3Si, and by the same argument, for Mo_3Si to convert to Mo.

These predictions are consistent with the above experimental results where, at the interface, Mo_5Si_3 formed. This interface would not be expected to convert to Mo_3Si and Mo if $MoSi_2$ is locally available, since the latter has a greater affinity for molec-

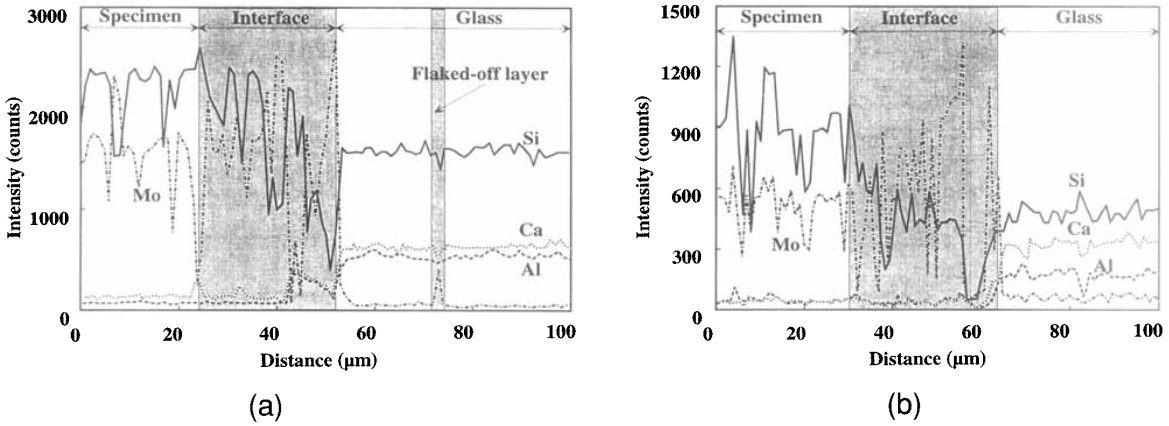

Fig. 6. Line EDS of molybdenum disilicide–glass interfacial region at (a) glass-line, (b) half-down regions.

when a critical thickness has been reduced to Mo_5Si_3, it dislodges from the interface and floats away as debris. No longer near regions of $MoSi_2$, local dissolved oxygen converts the Mo_5Si_3 to Mo_3Si, and Mo_3Si to Mo, which was observed by XRD in regions in the glass extended away from the interface.

The rate of corrosion was undoubtedly determined by the combined effects of the rates of coarsening of interfacial layers and the critical thicknesses at which interfacial stresses caused the coatings to crack and flake away, in turn, forcing new interfaces to form. Silicon diffusion through the Mo_5Si_3 is required to form vitreous silica, which dissolves into the glass. An appreciable volume percentage of silicon vacancies are expected to exist at the Mo_5Si_3 interface; as silicon removal from the lattice continues, silicon vacancies form until a structural collapse to a unit cell of different stoichiometry results. This is corroborated by the Si concentration gradiant shown by line EDS in Fig. 6. This type of interface would foster easy Si diffusion along these vacancy sites.

(3) $SiC_{(p)}/Al_2O_3$

Figures 8(a and b) show the $SiC_{(p)}/Al_2O_3$–glass interfacial features at the glass-line and half-down regions, respectively. Bubbles formed within the glass, near the composite surface at both the glass-line and half-down regions. Near the glass line, the bubbles are seen in contact with the bulk of the specimen. CO or CO_2 can be the product of reaction between SiC and oxygen, depending on oxygen activity.[13] Competing oxidation reactions are considered in Fig. 9. The SiC portion of the composite oxidizes most favorably, to form silica and carbon monoxide. Since the CO–CO_2 equilibria fall below the Richardson line (for Mo oxidation), the conversion of CO to CO_2 is not favorable, and the bubbles are expected to be purely carbon monoxide. Based on a standard Gibbs energy change of $\Delta G^{\circ}_{1823K} = -534.67$ kJ/mol, for the $SiC_{(s)}/CO_{(g)}$ equilibria, and a CO bubble pressure of 1 atm, the molecular oxygen activity for the equilibria is $a_{O_2} = 4.8 \times 10^{-16}$. Oxygen activities above this cause the reaction to be favorable.

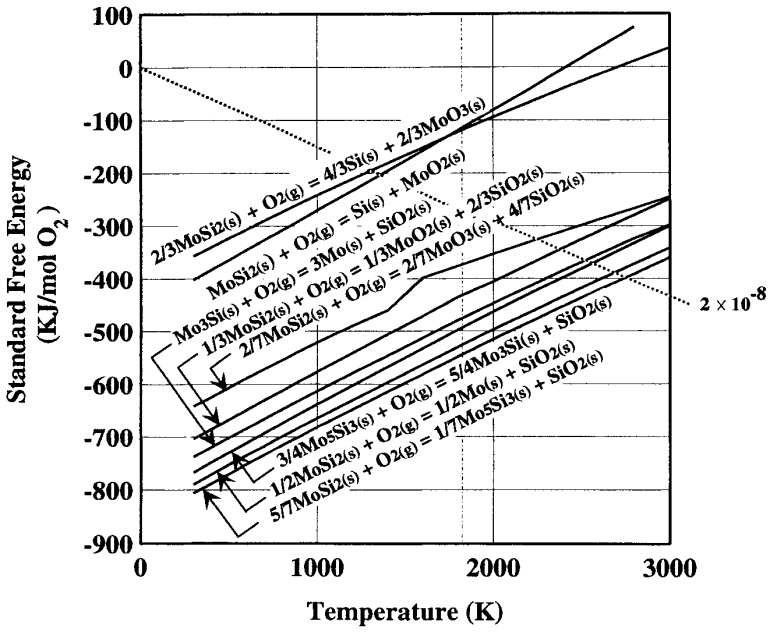

Fig. 7. Ellingham diagram of compounds of interest from $MoSi_2$–oxygen interaction. A Richardson line of 2.0×10^{-8} represents the highest possible molecular oxygen activity based on the results of Mo in E-glass. The dot–dashed line indicates the test temperature (1823 K). Thermody-

DOCKET ALARM

Explore Litigation Insights

Docket Alarm provides insights to develop a more informed litigation strategy and the peace of mind of knowing you're on top of things.

Real-Time Litigation Alerts

Keep your litigation team up-to-date with **real-time alerts** and advanced team management tools built for the enterprise, all while greatly reducing PACER spend.

Our comprehensive service means we can handle Federal, State, and Administrative courts across the country.

Advanced Docket Research

With over 230 million records, Docket Alarm's cloud-native docket research platform finds what other services can't. Coverage includes Federal, State, plus PTAB, TTAB, ITC and NLRB decisions, all in one place.

Identify arguments that have been successful in the past with full text, pinpoint searching. Link to case law cited within any court document via Fastcase.

Analytics At Your Fingertips

Learn what happened the last time a particular judge, opposing counsel or company faced cases similar to yours.

Advanced out-of-the-box PTAB and TTAB analytics are always at your fingertips.

API

Docket Alarm offers a powerful API (application programming interface) to developers that want to integrate case filings into their apps.

LAW FIRMS
Build custom dashboards for your attorneys and clients with live data direct from the court.

Automate many repetitive legal tasks like conflict checks, document management, and marketing.

FINANCIAL INSTITUTIONS
Litigation and bankruptcy checks for companies and debtors.

E-DISCOVERY AND LEGAL VENDORS
Sync your system to PACER to automate legal marketing.